# Some Aspects of the Structure of Convective Planetary Boundary Layers

J. C. WYNGAARD, S. P. S. ARYA[1] AND O. R. COTÉ

*Air Force Cambridge Research Laboratories, Bedford, Mass. 01730*

(Manuscript received 1 October 1973, in revised form 5 December 1973)

ABSTRACT

It is shown that although Coriolis forces cause large production rates of stress in a convective planetary boundary layer, there is a control mechanism involving mean wind shear which prevents stress levels from becoming large. Higher-order-closure model calculations are presented which show that the stress profiles are essentially linear, regardless of wind direction, providing the geostrophic wind shear vanishes and the wind speed jump across the capping inversion is negligible. It is shown that it will be very difficult to verify these predicted stress profiles experimentally because of averaging time problems. A simple two-layer model is developed which leads to geostrophic drag and heat transfer expressions in fairly good agreement with Wangara data.

## 1. Introduction

The structure of a stationary, horizontally homogenous, barotropic and non-stratified (neutral) Ekman layer has been thoroughly studied in recent years. There are available some elegant asymptotic arguments for its structural similarity (Blackadar and Tennekes, 1968), and recent numerical studies show the nature of the universal profiles of mean wind and turbulence levels (Deardorff, 1972; Wyngaard *et al.*, 1974). It is clear that in this simplified case, the boundary layer thickness scales with $u_*/f$, where $u_*$ is the so-called friction velocity and $f$ the Coriolis parameter.

The unstable boundary layer is, however, more controversial. While some investigators have maintained that the thickness is still tied to $u_*/f$ (see, e.g., Zilitinkevich, 1972; Clarke, 1970; Tennekes, 1970; Monin, 1970), recent model studies strongly suggest it is determined by $z_i$, the height of the lowest inversion base (Deardorff, 1972; Wyngaard *et al.*, 1974). These studies show that almost all the velocity and temperature differences across the boundary layer are confined to a thin region near the surface, which we will call the surface shear layer. In the essentially shear-free convective layer between this and $z_i$, the velocity and temperature fluctuations are found to scale with $w_*$ and $\theta_*$, defined by

$$\left.\begin{aligned} w_* &= \left(\frac{g}{T}Q_0 z_i\right)^{\frac{1}{3}} \\ \theta_* &= \left(\frac{Q_0^2 T}{g z_i}\right)^{\frac{1}{3}} \end{aligned}\right\}, \tag{1}$$

where $Q_0$ is the surface temperature flux, and $g/T$ the so-called buoyancy parameter.

The convective boundary layer, therefore, has $z_i$, the Obukhov length $L=-u_*^3T/(kQ_0g)$ and $u_*/f$ as characteristic lengths, so that distributions of flow properties should depend, in general, on $z/z_i$, $z_i/L$ and $u_*/(fz_i)$. The parameter $u_*/(fz_i)$ has not been varied much in the model experiments; Deardorff used a value of 2.2, while Wyngaard *et al.*, used 1.0. While there is no suggestion that its value affects turbulence structure, providing it is of the order of 1, it clearly is an important parameter for velocity defect profiles. This can be seen by starting from the equations of motion in dimensionless form:

$$\left.\begin{aligned} \frac{\partial(\overline{uw}/u_*^2)}{\partial(z/z_i)} &= \frac{fz_i}{u_*}\left(\frac{V-V_g}{u_*}\right) \\ \frac{\partial(\overline{vw}/u_*^2)}{\partial(z/z_i)} &= \frac{fz_i}{u_*}\left(\frac{U_g-U}{u_*}\right) \end{aligned}\right\}. \tag{2}$$

Here we have used a right-handed coordinate system with the $x$ axis in the direction of the mean surface wind $U$, and the $z$ axis vertical. The mean flow has components $U$ and $V$, $U_g$ and $V_g$ are those of the geostrophic flow, and $u$, $v$, $w$ are components of the fluctuating motion in the $x$, $y$, $z$ directions, respectively. After integrating Eqs. (2) and assuming that the stresses vanish at the top of the boundary layer, one obtains as integral constraints on the mean wind profiles

$$\left.\begin{aligned} \int_0^1 \left(\frac{V-V_g}{u_*}\right)\cdot\left(\frac{z}{z_i}\right) &= \frac{u_*}{fz_i} \\ \int_0^1 \left(\frac{U_g-U}{u_*}\right)\left(\frac{z}{z_i}\right) &= 0 \end{aligned}\right\}. \tag{3}$$

[1] Department of Atmospheric Sciences, University of Washington, Seattle 98195.

In the general case involving a jump in wind speed across the inversion at $z_i$ and significant wind shear above, the behavior of the wind and stress profiles within the convective layer is complex, as discussed by Deardorff (1973). We will consider here only the idealized case with negligible speed jump and wind shear in the inversion. As we show later, in this case the constraints (3) are satisfied in a simple manner. Within the convective layer the $\overline{nw}$ profile becomes linear, $\overline{vw}/u_*^2$ and $V/u_*$ vanish, and we have

$$\frac{V_g}{u_*}\approx\frac{u_*}{fz_i},\quad U\approx U_g. \tag{4}$$

The geostrophic adjustment in $V$ occurs within the inversion.

We show later that $u_*^2/w_*^2$ vanishes in the convective limit; thus, stress levels are far smaller than kinetic energy under typical conditions. Tennekes (1970) has also pointed this out, indicating that buoyant eddies support much less momentum transfer than their kinetic energy would seem to allow. The cause, he concludes, is the disparity of time scales of the buoyant and mechanical eddies which coexist in the convective layer. The buoyant eddies would greatly increase momentum transfer, he argues, were they tuned to the same frequency as the mechanical ones. The buoyant eddies are fast and energetic, with a time scale (in our notation) of $z_i/w_*$; the mechanical ones are weaker and slower, he says, with time scale of $f^{-1}$. Since these time scales can differ by an order of magnitude, this prevents strong interaction between buoyant and mechanical turbulence, he argues, and, hence, momentum transfer is not radically increased by convection.

Our explanation for the low stress levels in convective turbulence is quite different. By examining the balance equations, or budgets, of stress and the mean motion equations, we show that there is a control mechanism which tends to minimize stress profile curvature and keeps stress levels of order $u_*^2$. This control mechanism is effective when energy is put directly into the vertical velocity fluctuations (such as by buoyancy, for example) and does not depend on a difference in time scales. Because of the closure problem, we cannot prove this control hypothesis, but we will show that it seems to provide a coherent model of convective layer phenomena.

## 2. Maintenance of stress in the convective layer

Our starting point is the conservation equation for stress in the form appropriate for horizontally homogeneous, large Reynolds number turbulence (Wyngaard *et al.*, 1974):

$$\begin{aligned}\dot{\overline{u_iu_k}}+U_{i,j}\overline{u_ju_k}+U_{k,j}\overline{u_ju_i}+(\overline{u_iu_ju_k})_{,j}\\ =-(\overline{u_kp_{,i}}+\overline{u_ip_{,k}})+(\overline{u_k\theta}\delta_{3i}+\overline{u_i\theta}\delta_{3k})\frac{g}{T}\\ -2\tilde{\epsilon}\frac{\delta_{ik}}{3}-2\omega(\epsilon_{ijl}n_j\overline{u_lu_k}+\epsilon_{klm}n_l\overline{u_mu_i}).\end{aligned} \tag{5}$$

Here $u_i=(u,v,w)$ is the fluctuating velocity, $U_i=(U,V,0)$ the mean velocity, $p$ the fluctuating kinematic pressure, $\theta$ the fluctuating temperature, $n_i$ the unit vector along the earth's rotation axis, $\omega$ the rotation rate, $(\ )_{,j}$ represents $\partial(\ )/\partial x_j$, and the other notation is standard. Our interest is not in the details of this equation, but rather in its dominant terms averaged over the convective layer; accordingly, we disregard the fourth term on the left, a flux divergence term, since it averages to zero.

Consider the rotation terms in Eq. (5). Because of their structure, they bring contributions from both diagonal components (energies) and off-diagonal ones (stresses) into the stress equations, while only stresses enter the rotation terms in the energy equations. Energies are of order $w_*^2$ while stresses are of order $u_*^2$, and their ratio is

$$\frac{w_*^2}{u_*^2}\approx\left(-\frac{z_i}{L}\right)^{\frac{2}{3}}, \tag{6}$$

which is large since typical $-z_i/L$ values are in the 10–1000 range. It is immediately clear that rotation effects are much more important in the stress equations than in the energy equations. The dominant terms in the energy equations are of the order of the buoyant production rate, $gQ_0/T$, so there the rotation terms (of order $fu_*^2$) are negligible:

$$fu_*^2\Big/\frac{g}{T}Q_0=\frac{fu_*^2}{fw_*^2}\approx\left(-\frac{z_i}{L}\right)^{-\frac{2}{3}}. \tag{7}$$

In the stress budgets, on the other hand, the rotation terms are dominant; in fact, they are relatively larger than the dominant terms in the energy budgets. To see this, consider a time scale for energy:

$$\tau_e=\frac{\text{energy}}{\text{production rate}}\approx w_*^2\Big/\frac{g}{T}Q_0\approx\frac{z_i}{w_*}. \tag{8}$$

An analogous time scale for stress based on its rotational production rate is

$$\tau_s=\frac{u_*^2}{fw_*^2}=\frac{u_*}{fz_i}\left(-\frac{z_i}{L}\right)^{-\frac{1}{3}}\frac{z_i}{w_*}. \tag{9}$$

Here again, we meet the group $u_*/(fz_i)$. We will treat it as a constant of order 1, so from Eq. (9) $\tau_s$ becomes steadily smaller than $\tau_e$ as $-z_i/L$ increases. This raises the question of how the stress level is maintained at at $u_*^2$ in the face of such a large production rate; judging from the energy time scale, stress would be expected to be of order $u_*w_*$.

Another interesting point is the way the rotation production terms for stress change with coordinate rotation about the vertical. If we let the surface wind direction vary and keep the 1-direction along the wind, then the rotation terms [referred to the right side of

Eq. (5)] are as shown in Table 1. Note that the large input term changes sign and moves from one stress budget to another as the wind direction rotates a full circle. This raises the question of whether the structure of the convective boundary layer depends on the direction of the surface-layer wind.

The coupling between the stress budgets and the mean shear equations gives insight into these questions. The latter equations are simply the $z$-derivatives of the steady-state equations of mean motion, i.e.,

$$\frac{\partial^2\overline{uw}}{\partial z^2}=f\frac{\partial V}{\partial z},\quad \frac{\partial^2\overline{vw}}{\partial z^2}=-f\frac{\partial U}{\partial z}. \tag{10}$$

Using Eqs. (5) and (10), the shear production terms for stress are

$$\overline{uw}\text{:}\ -\overline{w^2}\frac{\partial U}{\partial z}=\frac{\overline{w^2}}{f}\frac{\partial^2\overline{vw}}{\partial z^2};\quad \overline{vw}\text{:}\ -\overline{w^2}\frac{\partial V}{\partial z}=-\frac{\overline{w^2}}{f}\frac{\partial^2\overline{uw}}{\partial z^2}. \tag{11}$$

Now consider the $\overline{uw}$ budget for west winds (that is, winds out of the west). From Table 1 the rotation term is of order $-fw_*^2$ and a source for negative $\overline{uw}$. In isolation, this would create large $\overline{uw}$ magnitudes at mid-levels, driving $\partial^2\overline{uw}/\partial z^2$ positive. From Eq. (11) this would introduce a large source of negative $\overline{vw}$ there, so $\partial^2\overline{vw}/\partial z^2$ would be driven positive. This puts a sink for negative $\overline{uw}$ into the $\overline{uw}$ equation, tending to balance the original rotational input term. A similar loop can be traced for different wind directions and for $\overline{vw}$. This is a control mechanism for stress levels; they cannot reach large magnitudes, say $u_*w_*$, because that would create stress profile curvature large enough to produce stress of the opposite sign and drive the level back to order $u_*^2$.

The stress profiles in the convective layer are determined by the balance of all terms in Eq. (5), including the very important pressure terms, but we suggest this control mechanism will limit the stress profile curvature and, hence, the deviations from linear stress profiles. In the next section, we discuss some results of model studies based in part on approximations to Eq. (5).

TABLE 1. Rotation terms in stress budgets for different wind directions and latitude $\phi$.

| Wind direction | Term | Order |
|---|---|---|
| | *$\overline{uw}$ budget* | |
| East | $-2\omega(\overline{u^2}\cos\phi-\overline{w^2}\cos\phi-\overline{vw}\sin\phi)$ | $fw_*^2$ |
| West | $2\omega(\overline{u^2}\cos\phi-\overline{w^2}\cos\phi+\overline{vw}\sin\phi)$ | $-fw_*^2$ |
| North | $2\omega(\overline{vw}\sin\phi+\overline{uv}\cos\phi)$ | $fu_*^2$ |
| South | $2\omega(\overline{vw}\sin\phi-\overline{uv}\cos\phi)$ | $fu_*^2$ |
| | *$\overline{vw}$ budget* | |
| East | $-2\omega(\overline{uw}\sin\phi+\overline{uv}\cos\phi)$ | $fu_*^2$ |
| West | $-2\omega(\overline{uw}\sin\phi-\overline{uv}\cos\phi)$ | $fu_*^2$ |
| North | $2\omega(\overline{v^2}\cos\phi-\overline{w^2}\cos\phi-\overline{uw}\sin\phi)$ | $-fw_*^2$ |
| South | $-2\omega(\overline{v^2}\cos\phi-\overline{w^2}\cos\phi+\overline{uw}\sin\phi)$ | $fw_*^2$ |

## 3. Model calculations

We have computed convective layer stress profiles with the model developed by Wyngaard *et al.* (1974). This model carries the exact mean shear equations (10) as well as the analogous $\partial\Theta/\partial z$ equation, and approximate forms of the $\overline{u_iu_k}$, $\overline{\theta u_i}$, $\overline{\theta^2}$ and $\bar{\epsilon}$ (energy dissipation rate) equations, a total of 14. The approximations, discussed in the original paper, deal with the flux divergence and pressure covariance terms. The pressure term approximations are most significant here. We used simple relaxation time forms, which are the leading terms in the expansions developed by Lumley and Khajeh-Nouri (1974). In the $\overline{uw}$ budget, for example, the pressure term was modeled as $-\overline{uw}/\tau$, with $\tau$ a time proportional to $q^2/\bar{\epsilon}$. Since equations for both $q^2$ (the turbulent kinetic energy) and $\bar{\epsilon}$ are carried, $\tau$ is determined by the system and in the convective layer is of order $z_i/w_*$. This makes the pressure term of order $fu_*w_*$, which cannot balance the rotation term of order $fw_*^2$. This modeling might not be correct in detail; rotation effects also cause pressure fluctuations, as discussed in the earlier paper, and, hence, they contribute directly to the pressure covariance. It is possible that the pressure term does have a component of order $fw_*^2$ due to rotation, and this could partially compensate directly the rotation inputs in the stress equations. Our model calculations are therefore "worst case" in terms of stress profile curvature and wind shear, because the model forces shear to be of order $f$ to balance the rotation terms in the stress equations; the true shear could be less. The model also treats the inversion at $z_i$ as a rigid lid, which is only a crude representation. As a result, we will concentrate only on the broad features of the calculated steady-state structure. All results are for 45N latitude.

The vertical profiles of most velocity and temperature variances and covariances are presented in the original paper. The linear profile of vertical heat flux was not mentioned there, but this follows immediately from the steady-state solution of the mean temperature gradient equation:

$$\frac{\partial}{\partial t}\frac{\partial\Theta}{\partial z}=0=-\frac{\partial^2\overline{\theta w}}{\partial z^2}. \tag{12}$$

Fig. 1 shows the computed $\overline{uw}$ and $\overline{vw}$ profiles for $-z_i/L=50$ and four different wind directions. All profiles are slightly curved, the most nearly linear being those for west winds. The stress profiles become asymptotically independent of $z_i/L$; calculations for this state are shown in Fig. 2, for $-z_i/L=1000$.

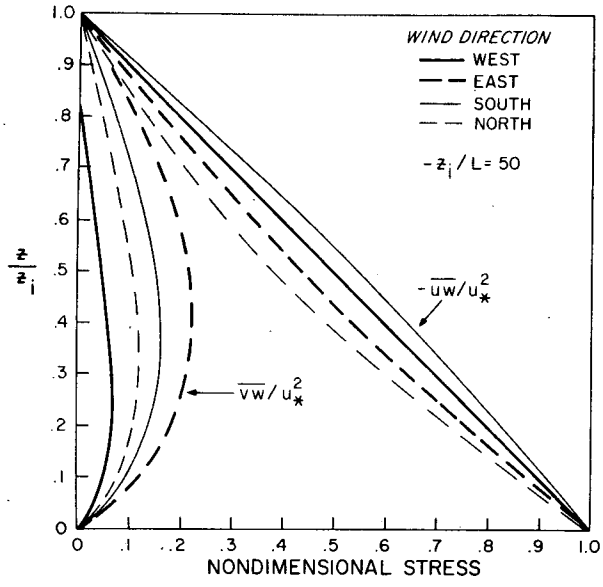


FIG. 1. Calculated stress profiles for the convective boundary layer at $-z_i/L=50$ for four wind directions.

Curves for $-z_i/L=500$ were the same, so the $-z_i/L$ dependence evidently vanishes around a few hundred.

The calculations indicate very small wind shears exist throughout the convective layer. Fig. 3 shows limiting velocity defect profiles for large $-z_i/L$ for east and west winds. The velocity difference across the entire convective layer is of the order of $u_*$. Note that for a west wind, both $\overline{uw}$ and $\partial U/\partial z$ are negative over most of the layer, so the eddy viscosity $K_m=-\overline{uw}/(\partial U/\partial z)$ is negative as well. The lateral wind magnitudes were very small, typically of the order of 0.1 $u_*$.

Any inaccuracies in these profile calculations are likely to be in the direction of overestimation of stress curvature and wind shear, so it appears that the convective layer structure does not depend significantly on wind direction. The simple expressions (4) are good approximations, and we will show they lead to a simple geostrophic drag law.

Thus far, we have considered the geostrophic wind to be independent of $z$, but we have also made calculations using linear profiles of geostrophic wind shear:

$$\frac{\partial U_g}{\partial z},\quad \frac{\partial V_g}{\partial z}=\pm 10f\left(1-\frac{z}{z_i}\right). \tag{13}$$

This gives an average magnitude of $5f$ over the convective layer, which at 45° latitude is $5\times10^{-4}$ sec$^{-1}$ or 0.5 m sec$^{-1}$ change in $U_g$ and $V_g$ per kilometer height, not a large value. The stress profiles are strongly affected, however, as shown in Figs. 4 and 5 for west winds and $-z_i/L=50$. The curvature introduced into the stress profiles can be explained through the mean shear equations, which now take the form

$$\left.\begin{aligned}\frac{\partial^2\overline{uw}}{\partial z^2}&=f\left(\frac{\partial V}{\partial z}-\frac{\partial V_g}{\partial z}\right)\\ \frac{\partial^2\overline{vw}}{\partial z^2}&=f\left(\frac{\partial U_g}{\partial z}-\frac{\partial U}{\partial z}\right)\end{aligned}\right\}. \tag{14}$$

Our layer-averaged values of $5f$ for the magnitudes of $\partial U_g/\partial z$ and $\partial V_g/\partial z$ are equivalent to $5u_*z_i$, since we set $z_i=u_*/f$ in the model. These values of geostrophic wind shear, although small, are larger than the wind shear in the convective layer, so the geostrophic terms in Eq. (13) dominate. In the Northern Hemisphere (and vice versa for the Southern Hemisphere), the

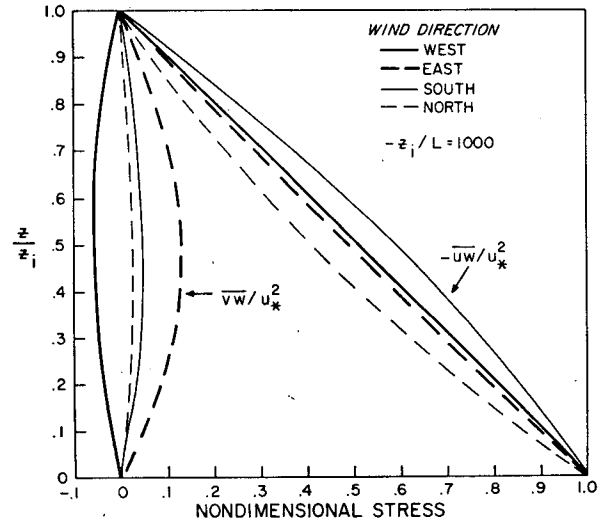


FIG. 2. Calculated stress profiles for the convective boundary layer in the convective limit ($-z_i/L$ larger than a few hundred) for four different wind directions.

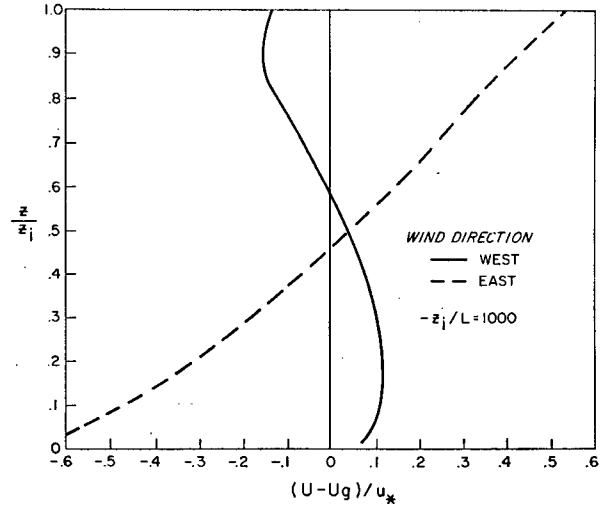


FIG. 3. Calculated velocity-defect profiles, in the convective limit, for east and west winds.

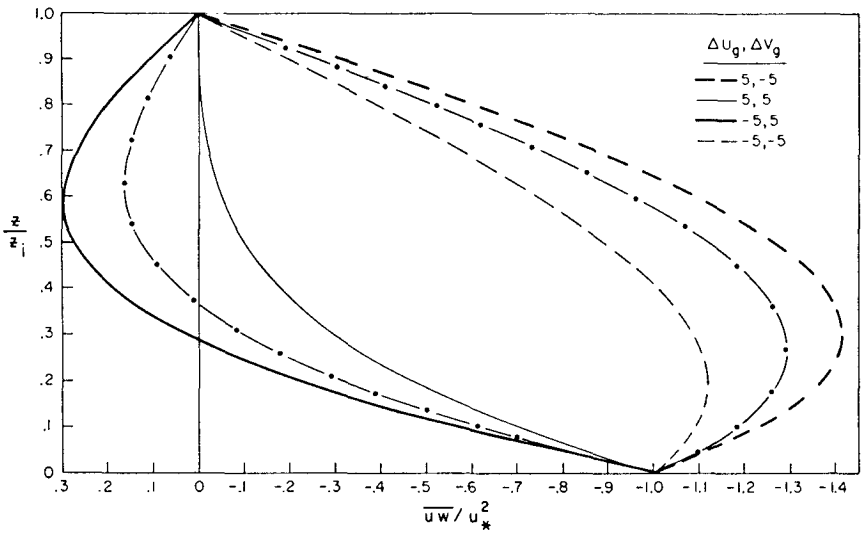


FIG. 4. Calculated $\overline{wu}$ profiles for four cases of geostrophic wind shear at $-z_i/L=50$. $\Delta U_g$, for example, is $[U_g(z_i)-U_g(0)]/u_*$, and the geostrophic shear profile is linear. The dot-dash curves are solutions of $(uw)_{,33}=-fV_{g,3}$.

curvature of $\overline{uw}$ then should be opposite in sign to $\partial V_g/\partial z$, while the curvature of $\overline{vw}$ should have the same sign as $\partial U_g/\partial z$. Figs. 4 and 5 confirm this and show also that the stress profiles are close to those predicted by keeping only the geostrophic wind shear terms on the right side of Eq. (13).

## 4. Can stress profiles be measured?

A typical convective boundary layer might have $z=1000$ m, $-L=10$ m, so $-z_i/L=100$. Since $w_*^2/u_*^2=(-z_i/L)^{2/3}$, energy levels will be much larger than stress. An experimenter wishing to compute stress directly from single-point measurements of velocity components will then be faced with the problem of determining the near-zero mean ($\sim u_*^2$) of a signal with large excursions ($\sim w_*^2$). It seems clear that for a given accuracy requirement, this will dictate increasingly longer averaging times as $-z_i/L$ grows.

The averaging time $T$ required to determine the time mean $f_T$ of any process $f$ to an accuracy $a$ (the error level divided by the mean) is (Lumley and Panof-

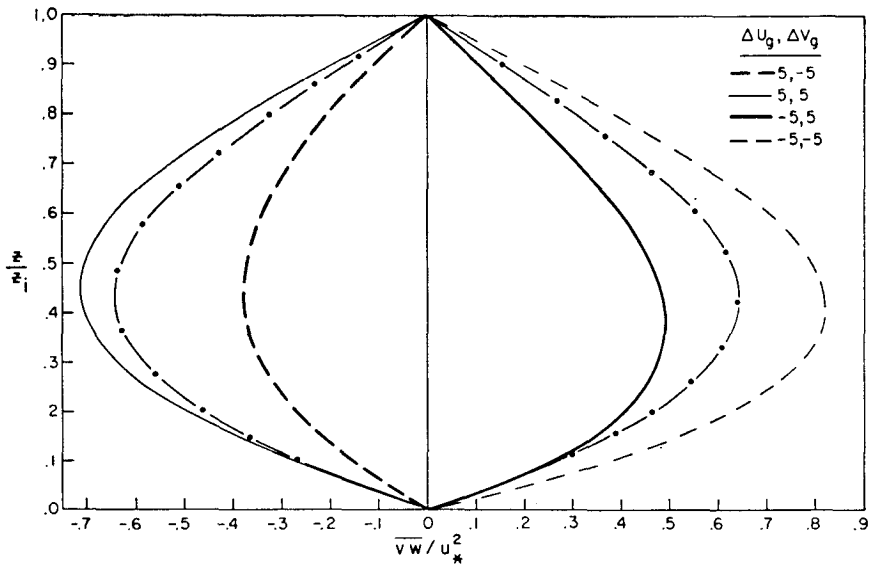


FIG. 5. Calculated $\overline{vw}$ profiles for the conditions of Fig. 4. The dot-dash curves are solutions of $(vw)_{,33}=fU_{g,3}$.

TABLE 2. Relative averaging times $T$ and accuracy $a$ at $z/z_i=0.5$.

| Statistic | Averaging time for fixed $a$ | Accuracy at fixed $T$ |
|---|---|---|
| Variances (e.g., $\overline{w^2}$) | 1 | 1 |
| Heat flux $\overline{w\theta}$ | 2 | 1.4 |
| Stress | | |
| $\overline{uw}$, $-z_i/L=10$ | 10 | 3 |
| $\overline{uw}$, $-z_i/L=100$ | 230 | 15 |

sky, 1964)

$$T\approx\frac{2\tau\overline{f'^2}}{\bar{f}^2a^2}, \tag{15}$$

where $\overline{f'^2}$ is the ensemble average variance of $f$ about its ensemble mean $\bar{f}$, and $\tau$ is the integral time scale of $f$. Wyngaard (1973) has shown with this formula that stress averaging times greatly exceed those for variances or heat flux in the unstable surface layer. We can extend those results to the convective layer at, say, $z/z_i=0.5$. We take $f$ to be $w^2$, $uw$, $w\theta$, and ask for the averaging time to determine their mean to a given accuracy. If we take the integral scale to be the same for all three signals, this time is proportional to $F_f=\overline{f'^2}/\bar{f}^2$. Since $F_f$ is determined by even moments whose major contributions are from the energy-containing eddies, we will use Gaussian predictions. For variances, we then have, using $w^2$ as an example,

$$F_{\overline{w^2}}=\frac{\overline{w^4}-(\overline{w^2})^2}{(\overline{w^2})^2}=K-1\approx 2, \tag{16}$$

where $K$, the kurtosis, is 3 for a Gaussian variable. For heat flux, we have

$$F_{\overline{w\theta}}=\frac{\overline{w^2\theta^2}-(\overline{w\theta})^2}{(\overline{w\theta})^2}\approx\frac{\overline{w^2}\,\overline{\theta^2}}{(\overline{w\theta})^2}+1. \tag{17}$$

At $z/z_i=0.5$, our model calculations give (Wyngaard *et al.*, 1974)

$$\begin{aligned}&\overline{w^2}\approx 0.4w_*^2,\quad \overline{w\theta}\approx 0.5w_*\theta_*,\\ &\overline{u^2}=\overline{v^2}\approx 0.15w_*^2,\\ &\overline{\theta^2}\approx 2\theta_*^2,\quad \overline{uw}\approx -0.5u_*^2,\end{aligned} \tag{18}$$

so that $F_{\overline{w\theta}}\approx 4$. This indicates factor of 2 longer averaging times for heat flux than for variances. For $\overline{uw}$, we have

$$F_{\overline{uw}}=\frac{\overline{u^2w^2}-(\overline{uw})^2}{(\overline{uw})^2}\approx\frac{\overline{u^2}\,\overline{w^2}}{(\overline{uw})^2}+1. \tag{19}$$

Using the results (18) this becomes

$$F_{\overline{uw}}\approx 0.24\left(\frac{w_*}{u_*}\right)^4\approx\left(-\frac{z_i}{L}\right)^{4/3}, \tag{20}$$

which is much larger than for variances or heat flux. We must therefore expect much longer averaging times for stress.

For fixed averaging times, the scatter $a$ in the time averages will vary as $F_f^{1/2}$, from Eq. (15), so we must also expect much more scatter in stress measurements than in variances or heat flux. Table 2 summarizes the situation, using variance measurements as a reference, and suggests that stress cannot be measured accurately enough from fixed-point sensors to test our model predictions. Remote probing or aircraft measurements seem required.

## 5. Geostrophic drag and heat transfer relations

The model calculations indicate that for $-z_i/L$ larger than 5 or 10, and in the absence of geostrophic wind shear, an essentially shear-free convective layer exists with $U=U_g$ and $V=0$. Above the inversion base $V\rightarrow V_g=u_*^2/(fz_i)$, while $U=U_g$. We can construct a simple geostrophic drag model by ignoring the slight, wind-direction-dependent shears that do exist above the surface shear layer, and assuming that Monin-Obukhov similarity holds for the $\partial U/\partial z$ profile in this lower layer of thickness $h_s$. That is, assuming that $U=U_g$ at $z=h_s$, we have

$$\frac{U_g}{u_*}=\frac{1}{k}\left[\ln\left(\frac{h_s}{z_0}\right)-\psi_1\left(\frac{h_s}{L}\right)\right], \tag{21}$$

where $\psi_1$ is related to the dimensionless wind shear $\phi_m(z/L)=(kz/u_*)(\partial U/\partial z)$ (see, e.g., Paulson, 1970). Similarly, after integrating the dimensionless lapse rate $\phi_h(z/L)=(kz/T_*)(\partial\Theta/\partial z)$, one obtains

$$\frac{\Delta\Theta}{T_*}=\frac{0.74}{k}\left[\ln\left(\frac{h_s}{z_0}\right)-\psi_2\left(\frac{h_s}{L}\right)\right], \tag{22}$$

where $\Delta\Theta=\Theta_\infty-\Theta_0$ is the potential temperature difference across the boundary layer. The factor 0.74 in Eq. (22) is from the Kansas profile observations reported by Businger *et al.* (1971).

For fixed $z_i$ one expects $h_s$ to decrease with decreasing $-L$ (see also Webb, 1958), and as a first approximation we take

$$h_s=-a_1L. \tag{23}$$

The coefficient $a_1$ can be estimated from measured surface-layer wind and temperature profiles under very unstable conditions. After examining all such profiles taken from a 16 m tower during the Wangara expedition (Clarke *et al.*, 1971), when $-L$ was often as small as 1 m, and those published by Dyer and Hicks (1970), we

find that there is always some measurable wind shear up to the highest level (16 m) although it does decrease with $-L$. For one run, with $-L=0.4$ m, there was a slight reversal of wind shear between 8 and 16 m, but winds were light (2 m sec$^{-1}$) and highly variable. Webb (1958) examined temperature profiles to 30 m under strong convection and found that the height where $\partial\Theta/\partial z$ vanished decreases with increasing instability, falling below 8 m in the most unstable cases ($-L\leqslant 1$ m). This evidence suggests we can take $a_1$ of the order of 10.

Substituting from Eq. (23) into Eqs. (21) and (22), we have

$$\frac{U_g}{u_*}=\frac{1}{k}\left[\ln\left(-\frac{L}{z_0}\right)+C_1\right], \tag{24}$$

$$\frac{\Delta\Theta}{T_*}=\frac{0.74}{k}\left[\ln\left(-\frac{L}{z_0}\right)+C_2\right], \tag{25}$$

where $C_1$ and $C_2$ are constants dependent only on $a_1$. Using $\psi_1$ and $\psi_2$ as evaluated by Paulson (1970), we obtain

$$C_1=\ln\left[\frac{8a_1}{(1+b_1)^2(1+b_1^2)}\right]+2\tan^{-1}b_1-\frac{\pi}{2}, \tag{26}$$

$$C_2=\ln\left[\frac{4a_1}{(1+b_2)^2}\right], \tag{27}$$

where

$$\left.\begin{aligned} b_1&=(1+15a_1)^{\frac{1}{4}}\\ b_2&=(1+9a_1)^{\frac{1}{2}}\end{aligned}\right\}. \tag{28}$$

Following Businger *et al.* (1971), we have taken

$$\phi_m=\left(1-15\frac{z}{L}\right)^{-\frac{1}{4}} \quad \text{and} \quad \phi_h=0.74\left(1-9\frac{z}{L}\right)^{-\frac{1}{2}}.$$

These expressions were established from observations over a limited $-z/L$ range, and their unlimited extrapolation is unjustified for anything but crude estimates. They imply, through Eqs. (26) and (27), values of $C_1$ and $C_2$ as shown in Table 3. Note that $C_1$ and $C_2$ are not very sensitive to the value of $a_1$, and for practical purposes one can take $C_1=0$ and $C_2=-1.0$.

Since $V_g/u_*=u_*/(fz_i)$ and under typical conditions this is much less than $U_g/u_*$, to a good approximation we can take $G=U_g$. Our simple expressions then are

$$\frac{G}{u_*}=\frac{1}{k}\left[\ln\left(-\frac{L}{z_0}\right)\right], \tag{29}$$

TABLE 3. Constants in drag and heat transfer laws.

| | $a_1$ | | | | | |
|---|---|---|---|---|---|---|
| | 10 | 20 | 30 | 40 | 50 | 60 |
| $C_1$ | −0.20 | −0.01 | 0.08 | 0.14 | 0.19 | 0.95 |
| $C_2$ | −1.02 | −0.96 | −0.93 | −0.91 | −0.90 | −0.81 |

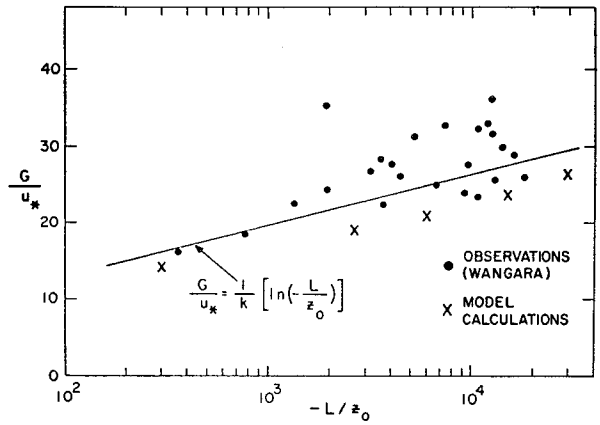


FIG. 6. Geostrophic drag observations and the model predictions.

$$\frac{\Delta\Theta}{T_*}=\frac{0.74}{k}\left[\ln\left(-\frac{L}{z_0}\right)-1.0\right]. \tag{30}$$

An expression essentially equivalent to Eq. (30) was derived also by Tennekes (1970), but he rejects Eq. (29) on the grounds that it depends too strongly on $L$.

Eqs. (29) and (30) are tested against the Wangara data in Figs. 6 and 7. Values of $G$ were found by smoothing the measured wind profiles just below the inversion, and $\Delta\Theta$ was taken as the difference between the potential temperature minimum just above the surface layer and the (extrapolated) potential temperature at $z_0$. The gradual increase in potential temperature above this minimum made it difficult to determine $\Theta_\infty$ any other way. The drag data (Fig. 6) agree fairly well with Eq. (29) and the model calculations, and seem to refute Tennekes' claim that Eq. (29) has excessive $L$-dependence. The temperature data (Fig. 7) are consistently higher than both the model calculations and Eq. (30). The difference is an additive constant of the order of 5–10; the stability trend does seem to agree with the predictions.

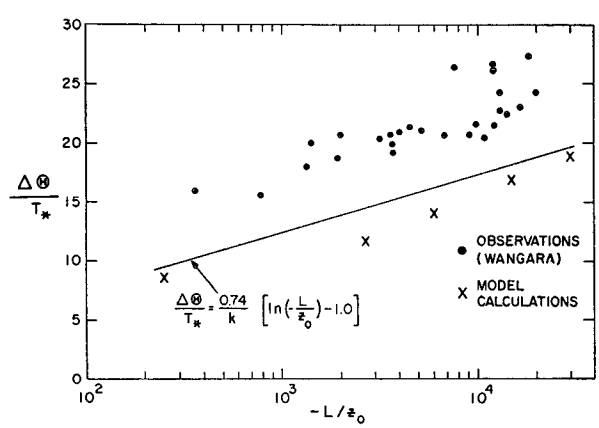


FIG. 7. Temperature difference observations and the model predictions.

## 6. Conclusions

The role played by rotational production terms in the budget equations for the second moments (variances and turbulent fluxes) is examined for the convective planetary boundary layer. Order-of-magnitude estimates of the rotation terms indicate that they are very important in the stress equations. Since their magnitudes and signs change with coordinate rotation about the vertical, this raises the possibility that the structure of a convective boundary layer depends on the wind direction. The numerical modeling computations by Deardorff (1972) and Wyngaard *et al.* (1974) were carried out only for west winds and therefore shed no light on this, but they did indicate, among other things, essentially linear stress profiles for $-z_i/L$ greater than 5 or 10.

It is argued that there is a control mechanism involving mean shears which prevents any significant deviation of the stress profiles from linearity, regardless of wind direction, even in the face of a very large rotational production terms. This is further supported by numerical calculations [using the higher-order-closure model of Wyngaard *et al.* (1974)] of the stress profiles for different wind directions. The most nearly linear profiles are for west winds; those for other wind directions are slightly curved. However, they all become asymptotically independent of $-z_i/L$ at large values of this parameter. The results indicate very small wind shears throughout the convective layer.

Since any inaccuracies in the model calculations are likely to be in the direction of overestimation of stress profile curvature and wind shear, it seems that convective layer structure does not depend significantly on wind direction. In the asymptotic limit of large instability ($-z_i/L > 5$–$10$), this leads to simple expressions for the geostrophic drag and heat transfer coefficients.

*Acknowledgments*. We would like to thank Profs. H. A. Panofsky and J. A. Businger for many helpful discussions and Prof. R. G. Fleagle for inviting the senior author to the Department of Atmospheric Sciences, University of Washington, for three months, during which much of this work was carried out. Our thanks are also due to Mr. R. Sizer for preparing the drawings and Mrs. Jo Ann Jarrett for typing this manuscript. Partial support of the National Science Foundation under Grant 14680 is also acknowledged.

### REFERENCES

Blackadar, A. K., and H. Tennekes, 1968: Asymptotic similarity in neutral barotropic planetary boundary layers. *J. Atmos. Sci.*, **25**, 1015–1020.

Businger, J. A., J. C. Wyngaard, Y. Izumi and E. F. Bradley, 1971: Flux-profile relationships in the atmospheric surface layer. *J. Atmos. Sci.*, **28**, 181–189.

Clarke, R. H., 1970: Observational studies in the atmospheric boundary layer. *Quart. J. Roy. Meteor. Soc.*, **96**, 91–114.

——, A. J. Dyer, R. R. Brook, D. G. Reid and A. J. Troup, 1971: The Wangara experiment: Boundary layer data. Paper No. 19, Division of Meteorological Physics, CSIRO, Australia.

Deardorff, J. W., 1972: Numerical investigation of neutral and unstable planetary boundary layers. *J. Atmos. Sci.*, **29**, 91–115.

——, 1973: An explanation of anomalously large Reynolds stresses within the convective planetary boundary layer. *J. Atmos. Sci.*, **30**, 1070–1076.

Dyer, A. J., and B. B. Hicks, 1970: Flux-gradient relationships in the constant flux layer. *Quart. J. Roy. Meteor. Soc.*, **96**, 715–721.

Lumley, J. L., and B. Khajeh-Nouri, 1974: Computational modeling of turbulent transport. To appear in *Advances in Geophysics*.

Monin, A. S., 1970: The atmospheric boundary layer. *Rev. Fluid Mech.*, **2**, 225–250.

Paulson, C. A., 1970: The mathematical representation of wind speed and temperature profiles in the unstable atmospheric surface layer. *J. Appl. Meteor.*, **9**, 857–861.

Tennekes, H., 1970: Free convection in the turbulent Ekman layer of the atmosphere. *J. Atmos. Sci.*, **27**, 1027–1034.

Webb, E. K., 1958: Vanishing potential temperature gradients in strong convection. *Quart. J. Roy. Meteor. Soc.*, **84**, 118–125.

Wyngaard, J. C., 1973: On surface layer turbulence. *Workshop in Micrometeorology*, D. A. Haugen, Ed., Boston, Amer. Meteor. Soc., 101–149.

——, O. R. Coté and K. S. Rao, 1974: Modeling the atmospheric boundary layer. To appear in *Advances in Geophysics*.

Zilitinkevich, S. S., 1972: On the determination of the height of the Ekman boundary layer. *Boundary-Layer Meteor.*, **3**, 141–145.